

Magnetic field distribution in steel objects with different properties of hardened layer

A.V. Byzov*, D.G. Ksenofontov, V.N. Kostin and O.N. Vasilenko

Department of nondestructive testing, M.N. Miheev Institute of Metal Physics of Ural Branch of Russian Academy of Sciences, 18 Sof'i Kovalevskoy St, Ekaterinburg, 620108, Russia

(Received July 23, 2021, Revised September 13, 2021, Accepted October 15, 2021)

Abstract. A simulation study of the distribution of magnetic flux induced by a U-shaped electromagnet into a two-layer massive object with variations in the depth and properties of the surface layer has been carried out. It has been established that the hardened surface layer “pushes” the magnetic flux into the bulk of the magnetized object and the magnetic flux penetration depth monotonically increases with increasing thickness of the hardened layer. A change in the thickness and magnetic properties of the surface layer leads to a redistribution of magnetic fluxes passing between the poles of the electromagnet along with the layer and the bulk of the steel object. In this case, the change in the layer thickness significantly affects the magnitude of the tangential component of the field on the surface of the object in the interpolar space, and the change in the properties of the layer affects the magnitude of the magnetic flux in the magnetic “transducer-object” circuit. This difference in magnetic parameters can be used for selective testing of the surface hardening quality. It has been shown that the hardened layer pushes the magnetic flux into the depth of the magnetized object. The nominal depth of penetration of the flow monotonically increases with an increase in the thickness of the hardened layer.

Keywords: bulk; hardware-software system of magnetic testing; layer; magnetic flux; simulation; surface hardening

1. Introduction

Surface hardening of steel products is a widespread way to increase their wear resistance and resistance to fatigue fracture (Bunshan 2001, Davis 2002, Stepanova 2009, Santoshkumar *et al.* 2020). The presence of hardened layer of a single part is able to increase its lifetime, and subsequently increase in lifetime of whole structure. Moreover, it allows us to use more cheap alloys instead of expensive ones (Čiuplys *et al.* 2010).

The hardened layer is a zone with high and constant hardness, which completely consist of martensite. Besides in a process of hardening treatment a transition layer is formed between base metal and hardened layer and it contains phases concerning of both of base metal and hardened layer: martensite, bainite, pearlite, and ferrite (Prisco 2018).

* Corresponding author, junior researcher, E-mail: byzovav@imp.uran.ru

^aJunior researcher, E-mail: ksenofontov@imp.uran.ru

The thickness of the surface-hardened layers can vary over a very wide range: 0.2-1.0 mm - after laser heating; 1.5-3 mm for structures subject to fatigue wear, 10-20 mm and more - for products that must withstand increased contact loads (for example, track rollers, cold rolling rolls). Also due to the hardening the hardness of surface layer can be 2 times higher than the hardness of a base metal.

Generally speaking, values and physical properties of layers extremely depends on treatment conditions, composition of steel, its initial microstructure, residual stresses (Prisco 2018, Čiuplys *et al.* 2010).

Basically, methods of surface hardening are divided into two types: physical and chemical. Physical methods are related to the exposure of physical fields to raw material with point to reform the structure of material in the near surface zone. Chemical methods are aimed to inject new atoms in material from surrounding atmosphere and, subsequently, to hard the lattice due to appearing defects. The influence of vacuum carburization is discussed in (Sugimoto 2017). It is noted, that this technique leads to formation a large amount of retained austenite. Herein, carbon potential influence to the amount of retained austenite and hardness of surface layer.

Explosion hardening is intensively used for hardening of manganese steels (Ba *et al.* 2018, Zhang *et al.* 2010, Gao *et al.* 2021, Ba *et al.* 2020). After explosion reached depth of the layer can be equal to 35-40 mm. Moreover, process of hardening occurs in different depths on various mechanism: nanoscale deformation twin and dislocation hardening mechanism in the surface layer and dislocation hardening mechanism in the subsurface layer. Also review of the literature gives some other methods, among them: laser hardening (Sun *et al.* 2014, Tewary *et al.* 2014, Sundqvist *et al.* 2018), electromechanical hardening (Fedorova *et al.* 2017, Dudkina 2020, Dykha *et al.* 2019), and, for example, plasma hardening (Guo *et al.* 2020, Rakhadilov *et al.* 2020, Xiang *et al.* 2017).

In order to estimate the depth and properties of hardened layer there is a number of techniques. Acoustic methods (Baev *et al.* 2010, Baqeri *et al.* 2012, Salchak *et al.* 2015) are used when there is a pronounced boundary between the hardened layer and the core and when the layer thickness is greater than the ultrasonic wavelength. Eddy current methods (Cuffe *et al.* 2008, Kashefi and Kahrobaee 2013, Kahrobaee and Karimi 2019) are used to determine small (1-2 mm) thicknesses of surface hardening.

Also, there is method when defect of hardened layer can be detected by determination of surface friction coefficient (Kushida *et al.* 2014, Tressia *et al.* 2021) or with the help of Barkhausen magnetic noise methods (Sackmann *et al.* 2020).

Regarding magnetic methods it should note the works (He *et al.* 2017, Liu *et al.* 2017), in which the depth of layer is estimated by hysteresis loop techniques. Also, in (Shcherbinin and Gorkunov 1996) the method of local measurement (with the help of an attached transducer) of the average coercive force over the “magnetized volume” is described, which has figured out the most widespread practical use. However, the concept of “magnetized volume” is vague. It is unclear how the magnetic flux density changes with depth depending on the thickness and properties of the hardened layer.

The aim of this work is to study the distribution of a magnetic flux induced by a U-shaped electromagnet into a two-layer massive object with variations in the depth and properties of the hardened layer via finite element simulation.

2. Methodology of simulation

The simulation was carried out with help of numerical solution of the Maxwell equations system by the finite element method using the FEMM program (<https://www.femm.info/wiki/HomePage> 2021). FEMM addresses some limiting cases of Maxwell's equations. The magnetics problems addressed are those that can be considered as "low frequency problems," in which displacement currents can be ignored. Displacement currents are typically relevant to magnetics problems only at radio frequencies. In a similar vein, the electrostatics solver considers the converse case in which only the electric field is considered and the magnetic field is neglected.

Magnetostatic problems are problems in which the fields are time-invariant. In this case, the field intensity (H) and flux density (B) must obey:

$$\nabla \times \mathbf{H} = \mathbf{J} \quad (1.1)$$

$$\nabla \cdot \mathbf{B} = 0 \quad (1.2)$$

subject to a constitutive relationship between B and H for each material:

$$\mathbf{B} = \mu \mathbf{H} \quad (1.3)$$

If a material is nonlinear (e.g. saturating iron or alnico magnets), the permeability μ is actually a function of B:

$$\mu = \frac{\mathbf{B}}{\mathbf{H}(\mathbf{B})} \quad (1.4)$$

FEMM goes about finding a field that satisfies (1.1)-(1.3) via a magnetic vector potential approach. Flux density is written in terms of the vector potential, A, as:

$$\mathbf{B} = \nabla \times \mathbf{A} \quad (1.5)$$

Now, this definition of B always satisfies (1.2). Then, (1.1) can be rewritten as:

$$\nabla \times \left(\frac{1}{\mu(\mathbf{B})} \nabla \times \mathbf{A} \right) = \mathbf{J} \quad (1.6)$$

For a linear isotropic material (and assuming the Coulomb gauge, $\nabla \cdot \mathbf{A} = 0$), Eq. (1.6) reduces to:

$$-\frac{1}{\mu} \nabla^2 \mathbf{A} = \mathbf{J} \quad (1.7)$$

FEMM retains the form of (1.6), so that magnetostatic problems with a nonlinear B-H relationship can be solved.

In the general 3-D case, A is a vector with three components. However, in the 2-D planar and axisymmetric cases, two of these three components are zero, leaving just the component in the "out of the page" direction. The advantage of using the vector potential formulation is that all the conditions to be satisfied have been combined into a single equation. If A is found, B and H can then be deduced by differentiating A. The form of (1.6), an elliptic partial differential equation, arises in the study of many different types of engineering phenomenon. There are a large number of tools that have been developed over the years to solve this particular problem.

Boundary conditions for magnetic problems come in varieties Dirichlet and Neumann. In Dirichlet type of boundary condition, the value of potential A or V is explicitly defined on the

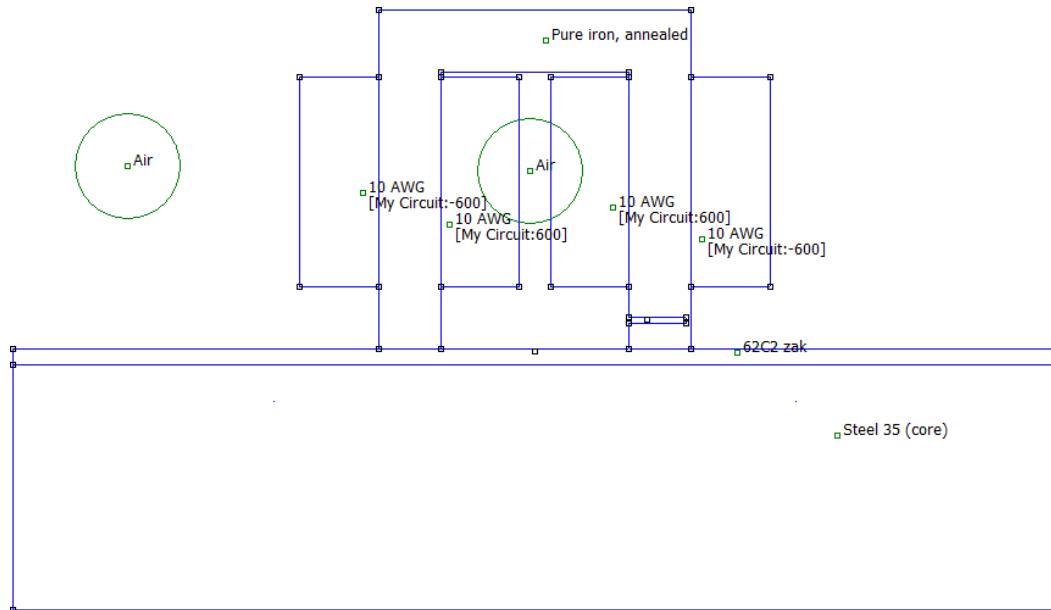


Fig. 1 Geometric model of the problem

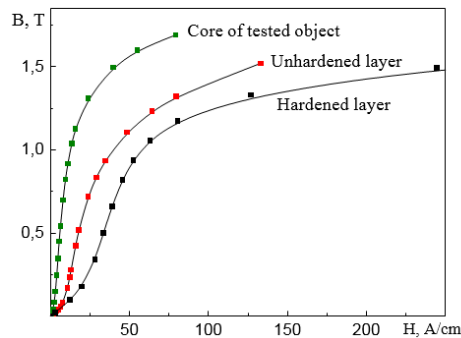


Fig. 2 Magnetization curves of materials used for simulation

boundary, e.g., $A = 0$. The most common use of Dirichlet-type boundary conditions in magnetic problems is to define $A = 0$ along a boundary to keep magnetic flux from crossing the boundary. In electrostatic problems, Dirichlet conditions are used to fix the voltage of a surface in the problem domain. In Neumann type boundary condition specifies the normal derivative of potential along the boundary. In magnetic problems, the homogeneous Neumann boundary condition, $\partial A / \partial n = 0$ is defined along a boundary to force flux to pass the boundary at exactly a 90° angle to the boundary. This sort of boundary condition is consistent with an interface with a very highly permeable metal. The geometric model of a two-layer tested object and an attached transducer is shown in Fig. 1. The problem was planar and its depth along z -axis was 28 mm. The dimensions of the magnetized object were 200x50 mm. The width of the poles of the electromagnet was 12 mm. Distance between poles was 36 mm. The magnetomotive force of the electromagnet was assumed constant and equal to 600 Ampere-turns.

In this study the properties of real materials were used (the magnetization curves in Fig. 2):

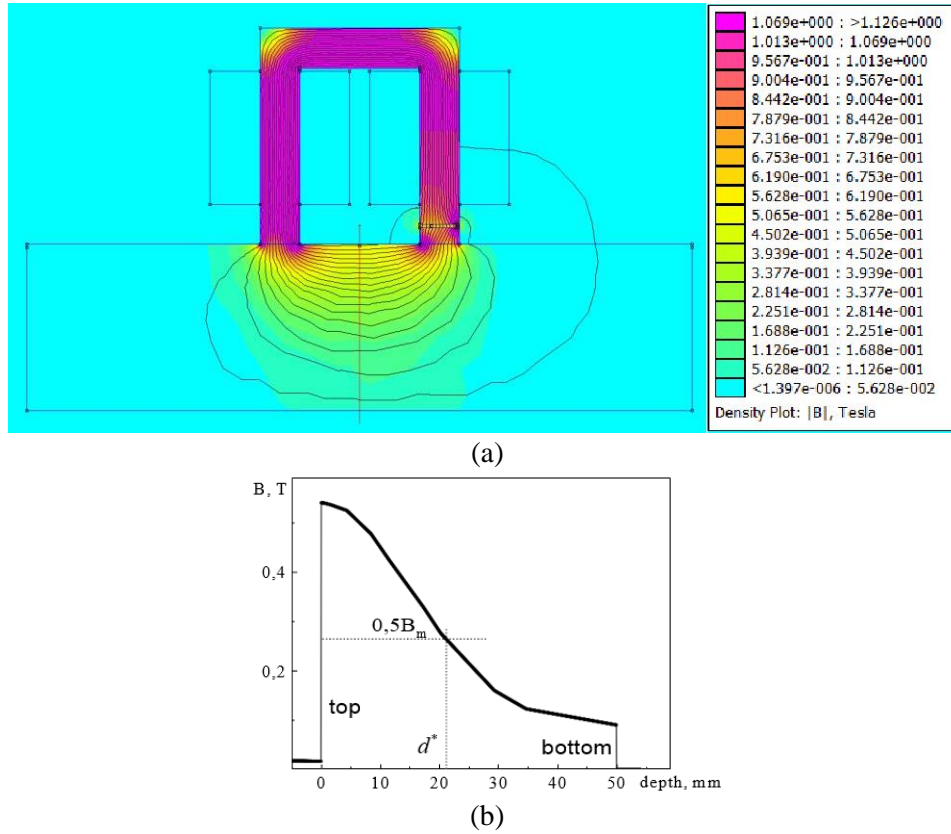


Fig. 3 Distribution of magnetic flux density in the “transducer-object” circuit (a) and along the depth of the object in the central section (b) in the absence of a hardened layer ($d_{lay} = 0$ mm)

unhardened core-steel 35 annealed at 850°C with a ferrite-pearlite structure (maximum magnetic permeability $\mu_{max} = 700$, strength of magnetic field of maximum magnetic permeability $H\mu_{max} = 800$ A/m); hardened layer - steel 62C2 hardened from 870°C with a martensitic structure ($\mu_{max} = 130$, $H\mu_{max} = 4800$ A/m); unhardened layer - annealed steel 40X with a ferrite-pearlite structure; electromagnet core-pure annealed iron.

3. Results

In Fig. 3 the distributions of the magnetic flux density (magnetic induction) in the magnetic “transducer-object” circuit (Fig. 3(a)) and along the depth of the object in the central cross section (Fig. 3(b)) in the absence of a hardened layer are shown. The figure shows that the magnetic flux density decreases monotonically from a value of $B_m = 0.54$ T on the upper face (surface) of the object to a value of $B = 0.09$ T on the lower face. The nominal penetration depth of magnetic flux d^* is assumed as the distance between the surface of the object and the depth where the flux density decreases 2 times from the maximum value of magnetic flux in the tested object without a hardened layer. As can be seen, in case of a homogeneous object d^* is equal to 21 mm.

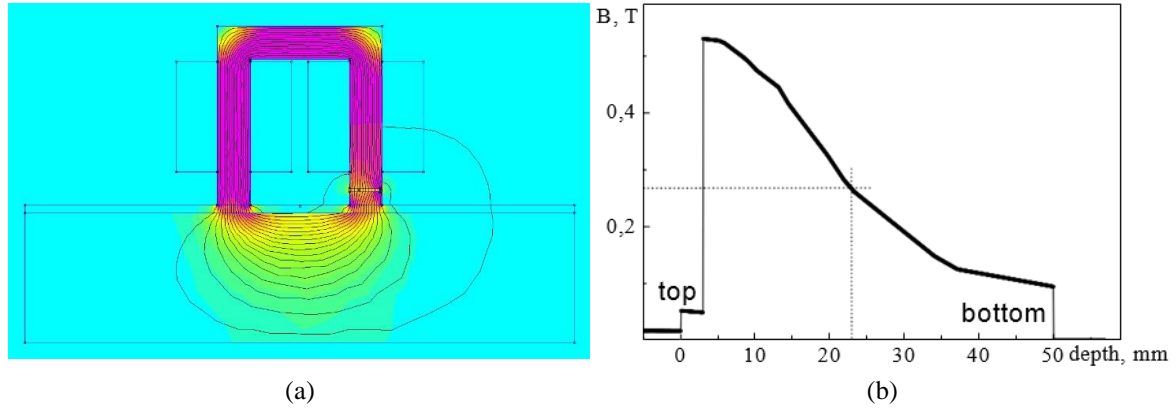


Fig. 4 Distribution of magnetic flux density in the “transducer-object” circuit (a) and along the depth of the object in the central section (b) with the thickness of the hardened layer $d_{lay} = 3$ mm

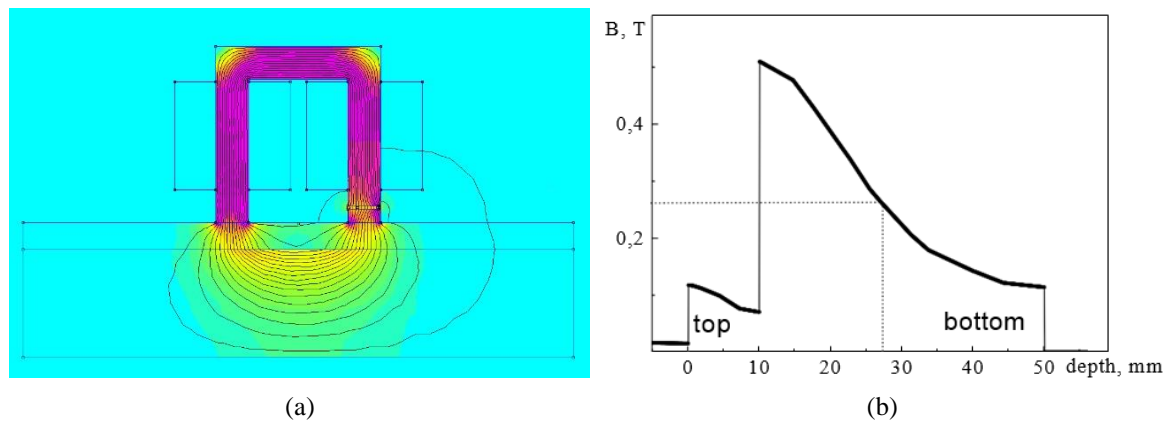


Fig. 5 Same as Fig. 4 with $d_{lay} = 10$ mm

Hardened layer. As can be seen from Fig. 4, the appearance of a hardened layer on the surface leads to the “pushing” of the magnetic flux into the depth of the object. The magnetic flux density in the hardened layer is 8 times less than in the upper layer of the soft magnetic core and 2 times less than on the lower surface of the object. Thus, almost whole magnetic flux induced by the electromagnet passes through the soft magnetic core. When the thickness of the hardened layer is equal to 3 mm, the nominal penetration depth of magnetic flux is equal to 22.5 mm.

As can be seen from Fig. 5, when the thickness of the hardened layer increases to 10 mm, the fraction of the magnetic flux passing through the hardened layer increases almost 2 times. However, the main part of the magnetic flow still passes through the unhardened core. In this case, the nominal penetration depth of magnetic flux increases to $d^* = 26$ mm.

A further increase in the thickness of the hardened layer leads to increase in the proportion and maximum density of the magnetic flux in the layer and to decrease in the flux in the core of the object. At = 20 mm (Fig. 6), the maximum values of the flux density in the layer and the core approach each other, but the maximum flux density in the core still exceeds the flux in the hardened layer. The nominal depth of penetration of the flow reaches the value $d^* = 33$ mm.

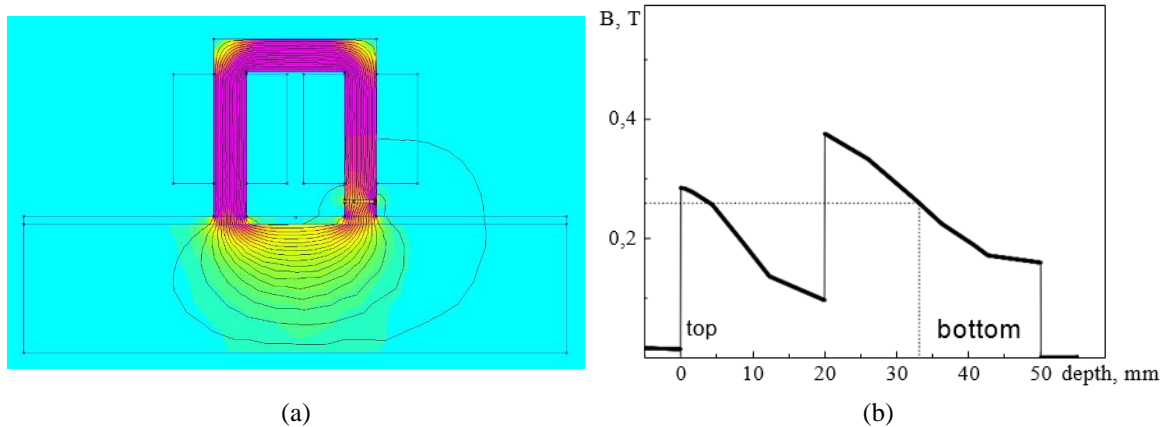


Fig. 6 Same as Fig. 4 with $d_{lay} = 20$ mm

Unhardened layer. For an insufficiently hardened layer, which has higher values of magnetic permeability and, consequently, lower values of magnetic resistance (Shcherbinin and Gorkunov 1996, Akhmedzhanov 2004), similar dependences are observed (Fig. 7-9).

When the layer depth changes from 0 to 20 mm, the nominal penetration depth of magnetic flux d^* increases from 21 to 31.5 mm. As can be seen from Fig. 9, at a depth of $d^* = 20$ mm, the maximum magnetic flux density in the layer is greater than in the core.

Thus, an increase in the thickness of the hardened layer, which differs from the core by lower values of the magnetic permeability, leads to a significant redistribution of magnetic fluxes passing through the layer and core, and an increase in the nominal penetration depth of magnetic flux. It is obvious that an increase in the magnetic flux density in the hardened layer should lead to an increase in the tangential component of the magnetic field H_x , which can be measured in the interpolar space of the electromagnet on the surface of the object under study (see Fig. 1). With an increase in the thickness of the hardened layer, the magnetic resistance of the “transducer-object” circuit should also increase, which can be determined by the magnitude of the normal component of the magnetic flux at the pole of the electromagnet B_y (Shcherbinin and Gorkunov 1996, Akhmedzhanov 2004). The value B_y should be additionally influenced by the magnetic permeability of the layer, which depends on the structure and degree of hardening (Stepanova 2009, Shcherbinin and Gorkunov 1996).

The values H_x and B_y can be measured using the DIUS-1.15M mobile hardware-software system described in (Kostin *et al.* 2018). In this case the value B_y is determined by the magnitude of the magnetic field in the transducer-hole of a special shape, made in the magnetic circuit of the electromagnet (see Fig. 1).

Fig. 10 shows the calculated dependencies of the field H_x and induction B_y for different thicknesses of the hardened (curve I) and unhardened (curve II) layers. As can be seen from curves I, both magnetic characteristics are sensitive to changes in the thickness of the hardened layer, but their sensitivities are very different. With an increase in depth to 40 mm, the H_x value increases by about 5 times, and the value decreases by 22%. Comparison of curves I and II shows that a change in the magnetic properties of the layer significantly affects the sensitivity of the H_x and B_y quantities to the layer thickness. These regularities can be used to selectively assess the depth of the layer and the degree of its hardening.

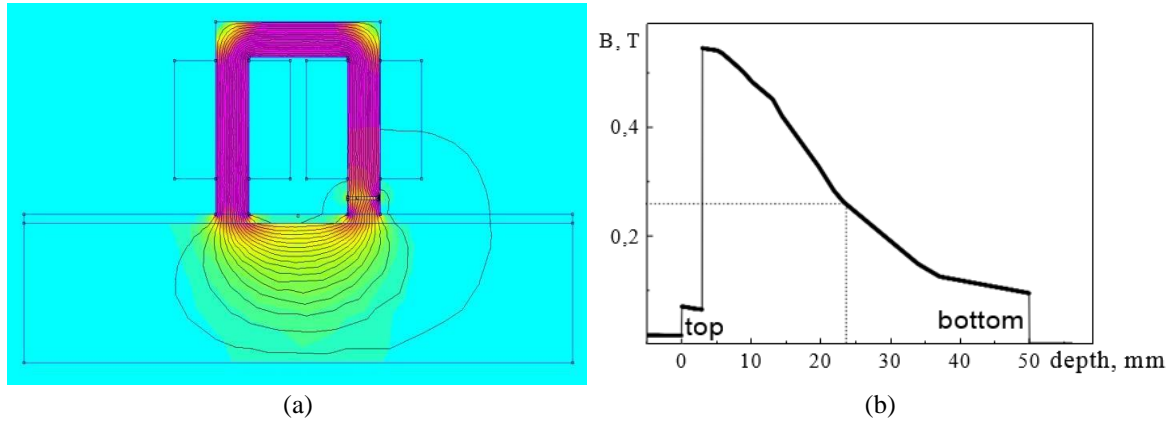


Fig. 7 Distribution of magnetic flux density in the “transducer-object” circuit (a) and along the depth of the object in the central section (b) with the thickness of the unhardened layer $d_{lay} = 3$ mm

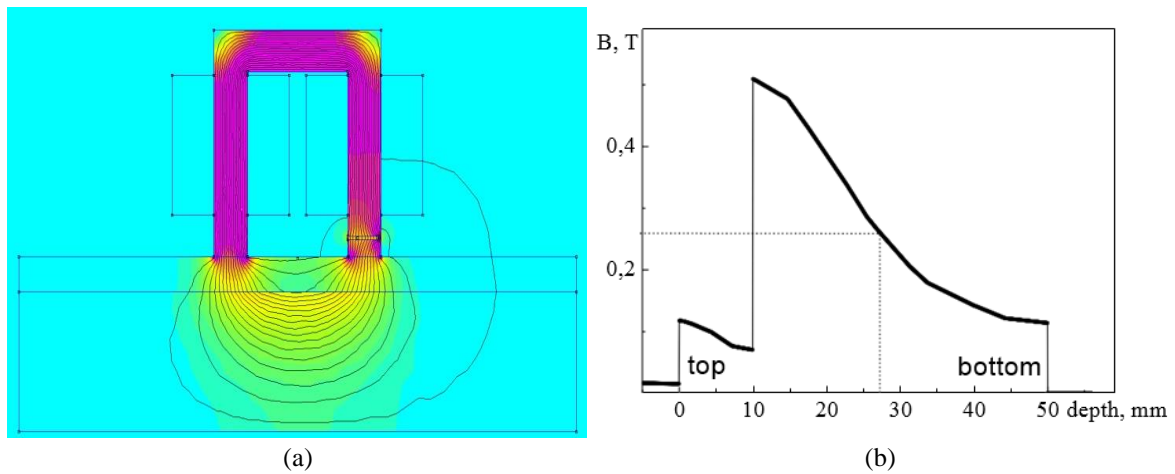


Fig. 8 Same as Fig. 7 with $d_{lay} = 10$ mm

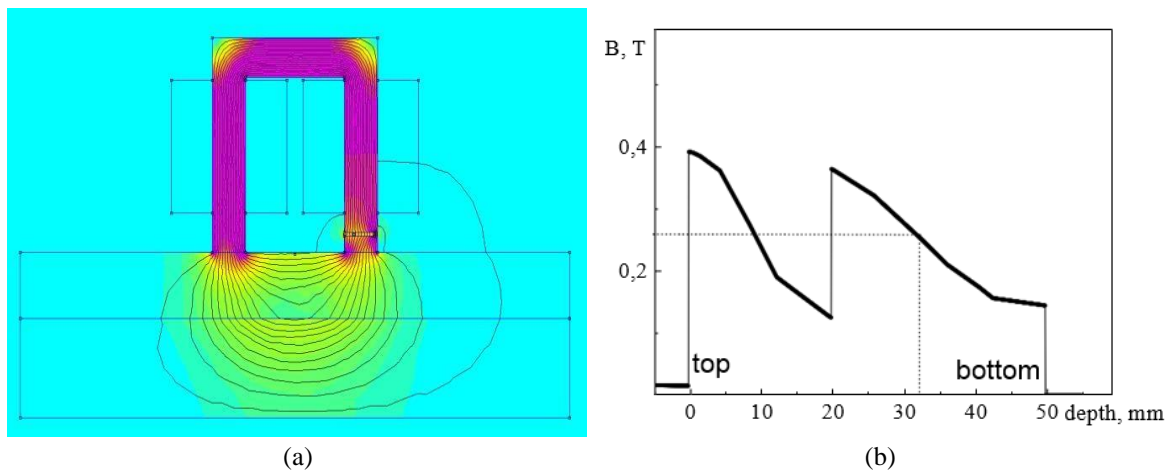


Fig. 9 Same as Fig. 7 with $d_{lay} = 20$ mm

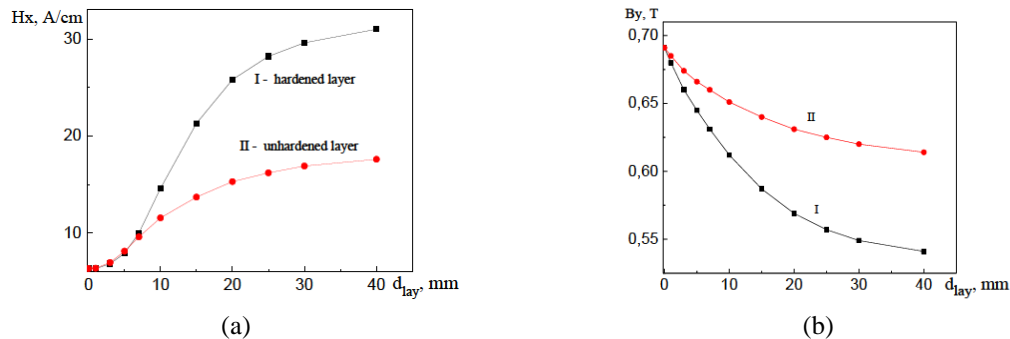


Fig. 10. Dependencies of H_x and B_y from thicknesses of hardened and unhardened layers

5. Conclusions

As a result of carrying out this study the following can be concluded:

- It has been shown that the hardened layer, which has a higher magnetic resistance in comparison with the core, pushes the magnetic flux into the depth of the magnetized object. The nominal depth of penetration of the flow monotonically increases with an increase in the thickness of the hardened layer.

- It has been found that with increasing thickness of hardened layer, the ratio of magnetic fluxes passing between the poles of the electromagnet along the hardened layer and the core changes. The magnetic flux in the layer increases several times and causes a monotonic growth of the tangential field component on the surface of the steel object.

- Due to the growth of the magnetic resistance with increasing, the value of the normal component of the magnetic flux at the pole of the electromagnet decreases. In addition, the measured value is significantly influenced by the value of the magnetic permeability of the layer depending on the degree of hardening.

The difference in the sensitivity of the quantities to changes in the thickness and physical properties of the hardened layer can be used to selectively assess the quality of surface hardening of steel products using the DIUS-1.15M hardware and software system (Kostin *et al.* 2018).

Acknowledgments

The research was carried out within the state assignment of Ministry of Science and Higher Education of the Russian Federation (topic “Diagnostics”, No. AAAA-A18-118020690196-3). D. Ksenofontov and A. Byzov are grateful to the M.N. Mikheev Institute of Metal Physics for support of their work on the state order of the Ministry of Education and Science of Russia on the topic “Diagnostics”, which was carried out within the framework of the youth project of the IMP UB RAS No. 22-21/mol.

References

Akhmedzhanov, R.A. (2004), *Phizicheskie Osnovy Magnitnogo Nerazrushayushchego Kontrolya* [Physical

- Fundamentals of Magnetic Non-destructive Testing], Omsk, Omsk State Trans. Univ., **69**. (in Russian)
- Baev, A.R., Majorov, A.L. and Tishchenko, M.A. (2010), "Ultrasonic methods of analysis of the metal articles surface hardening", *Litiyo i Metallurgiya [Found. Product. Metal.]*, **4**, 267-271. (in Russian)
- Ba, Q., Song, R., Feng, Y. and Li, L. (2018), "Microstructural properties and hardening mechanism of explosion hardening of Mn13Cr2 steel surface", *Adv. Mater. Process*, 487-494. https://doi.org/10.1007/978-981-13-0107-0_47.
- Ba, Q., Song, R., Zhou, N., Pei, Z., Feng, Y. and Song, R. (2020), "Revealing working hardening behavior and substructure evolutions of ultrahigh strength and enhanced wear resistance Fe-25Mn-7Al-1C steel treated by explosion processing", *J. Mater. Sci.*, **55**, 1256-1268. <https://doi.org/10.1007/s10853-019-04021-6>.
- Baqeri, R., Honarvar, F. and Mehdizad, R. (2012), "Case depth profile measurement of hardened components using ultrasonic backscattering method", *18th World Conference on Nondestructive Testing*, Durban, April.
- Bunshah, R.F. (2001), *Handbook of Hard Coatings, Deposition Technologies, Properties and Applications*, William Andrew Publishing, LLC, Norwich, New York, U.S.A.
- Čiuplys, V., Čiuplys, A., Vilys, J. and Kvedaras, V. (2010), "Increasing of carbon steel durability by surface hardening", *Mater. Sci.*, **16**(1), 24-28.
- Cuffe, J., Sun, H., Plotnikov, Y., Nath, S. and Sheila-Vadde, A. (2008), "Eddy current measurement of case hardened depth of steel components", *17th World Conference on Nondestructive Testing*, Shanghai, October.
- Davis, J.R. (2002), *Surface Hardening of Steels: Understanding the Basics*, ASM International, Cleveland, Ohio, U.S.A.
- Dudkina, N.G. (2020), "A study of the surface layer of steel 45 subjected to electromechanical treatment with pulsed deformation", *Metal Sci. Heat Treat.*, **62**(3-4), 259-262. <https://doi.org/10.1007/s11041-020-00545-w>.
- Dykha, A., Makovkin, O. and Dykha, M. (2019), "Influence of discrete electromechanical hardening on the wear resistance of steels", *Proceedings of the 2nd International Conference on Design, Simulation, Manufacturing: The Innovation Exchange DSMIE-2019*, Lutsk, June.
- Fedorova, L.V., Fedorov, S.K., Serzhant, A.A., Golovin, V.V. and Systerov, S.V. (2017), "Electromechanical surface hardening of tubing steels", *Metal Sci. Heat Treat.*, **59**(3), 173-175. <https://doi.org/10.1007/s11041-017-0123-z>.
- Finite Element Method Magnetics (2021), <https://www.femm.info/wiki/HomePage>
- Gao, T., Jin, X., Qiao, J., Yang, H., Zhang, Y. and Wu, Y. (2021), "Successive strain hardening mechanisms induced by transformation induced plasticity in Fe60Mn20Co10Cr10 high entropy alloys", *J. Appl. Phys.* **129**(175101), 1-10. <https://doi.org/10.1063/5.0041352>.
- Guo, D., Yu, D., Zhang, P., Duan, Y., Zhang, B., Zhong, Y. and Qiu, J. (2020), "Laminar plasma jet surface hardening of the U75V rail steel: Insight into the hardening mechanism and control scheme", *Surf. Coat. Tech.*, **394**(125857), 1-10. <https://doi.org/10.1016/j.surfcoat.2020.125857>.
- He, C., Yang, M., Liu, X., Wang, X. and Wu, B. (2017), "Characterisation of case depth in induction-hardened medium carbon steels based on magnetic minor hysteresis loop measurement technique", *Philos. Mag.*, **97**(31), 2829-2844. <https://doi.org/10.1080/14786435.2017.1355116>.
- Kahrobaee, S. and Karimi, E.Z. (2019), "Characterization of work-hardening in Hadfield steel using non-destructive eddy current method", *Nondestruct. Test. Eval.*, **34**(2), 178-192. <https://doi.org/10.1080/10589759.2019.1581190>.
- Kashefi, M. and Kahrobaee, S. (2013), "Dual-Frequency Approach to Assess Surface Hardened Layer Using NDE Technology", *J. Mater. Eng. Perform.*, **22**(4), 1108-1112. <https://doi.org/10.1007/s11665-012-0369-y>.
- Kostin, V.N., Vasilenko, O.N. and Byzov, A.V. (2018), "DIUS-1.15M mobile hardware-software structuroscopy system", *Russ. J. Nondestruct.*, **54**(9), 654-957. <https://doi.org/10.1134/S1061830918090048>
- Kushida, H., Maeda, Y., Kakimoto, H., Ishikawa, T. and Sugyo, S. (2014), "Surface defect generation

- behavior of wire rolling – analytical study of rolling conditions and experimental verification of surface-hardened layer”, *Tetsu-to-Hagané*, **100**(12), 103-109. <https://doi.org/10.2355/tetsutohagane.100.1535>.
- Liu, X., Zhang, R., Wu, B., Wang, X. and He, C. (2017), “Characterization and detection method for case depth evaluation based on magnetic hysteresis model of multi-layered structures”, *J. Mech. Eng.*, **53**(20), 7-12. <https://doi.org/10.3901/JME.2017.20.007>.
- Lo, C.C.H., Kinser, E.R. and Jiles, D.C. (2006), “Magnetic non-destructive characterization of case depth in surface-hardened steel components”, *AIP Conference Proceedings*, **820**, 1253-1260. <https://doi.org/10.1063/1.2184668>.
- Murikov, S.A., Artem’ev, I.A., Murikov, E.S., Kudryashov, A.A., Urtsev, V.N., Nichipuruk, A.P. and Stashkov, A.N. (2011), “Roller diagnostics in hot-rolling mills on the basis of the coercive force”, *Steel Transl.*, **41**(11), 954-957. <https://doi.org/10.3103/S0967091211110167>.
- Prisco, U. (2018), “Case microstructure in induction surface hardening of steels: an overview”, *Int. J. Adv. Manuf. Tech.*, **98**, 2619-2637. <https://doi.org/10.1007/s00170-018-2412-0>.
- Rakhadilov, B.K., Buranich, V.V., Satbayeva, Z.A., Sagdoldina, Z.B., Kozhanova, R.S. and Pogrebnyak, A.D. (2020), “The cathodic electrolytic plasma hardening of the 20Cr2Ni4A chromium-nickel steel”, *J. Mater. Res. Tech.*, **9**(4), 6969-6976. <https://doi.org/10.1016/j.jmrt.2020.05.020>.
- Sackmann, D., Heinzl, J. and Karpuschewski, B. (2020), “An approach for a reliable detection of grinding burn using the Barkhausen noise multi-parameter analysis”, *Procedia CIRP*, **87**, 415-419.
- Salchak, Y.A., Sednev, D.A., Kroening, M. and Ardashkin, I.B. (2015), “Method of case hardening depth testing by using multifunctional ultrasonic testing instrument”, *IOP Conf. Series: Mater. Sci. Eng.*, **81** (012080), 1-8. <https://doi.org/10.1088/1757-899X/81/1/012080>.
- Wagha, S.V., Bhatt, D.V., Menghanic, J.V. and Bhavikattid, S.S. (2020), “Effects of laser hardening process parameters on hardness depth of Ck45 steel using Taguchi’s optimization technique”, *IOP Conf. Series: Mater. Sci. Eng.*, **810**(012027), 1-9. <https://doi.org/10.1088/1757-899X/810/1/012027>.
- Shcherbinin, V.E. and Gorkunov, E.S. (1996), *Magnitnye Metody Strukturnogo Analiza I Nerazrushayushchego Kontrolya (Magnetic methods of structure analysis and nondestructive testing)*, Ekaterinburg, UrB RAS, 266. (in Russian)
- Stepanova, T.Y. (2009), *Tekhnologii Poverkhnostnogo Uprochneniya Detaley Mashin (Technologies of Surface Hardening of Machine Elements)*, Ivanovo, Ivanovskii Gos. Chem.-Tech. Univ., 64. (in Russian)
- Sugimoto K., Hojo T. and Mizuno Y. (2018), “Surface-hardened Layer Properties of Newly Developed Case Hardening Steel”, *ISIJ Int.*, **58**(4), 727-733. <https://doi.org/10.2355/isijinternational.ISIJINT-2017-460>.
- Sugimoto, K., Hojo, T. and Mizuno, Y. (2018), “Effects of vacuum-carburizing conditions on surface-hardened layer properties of transformation-induced plasticity-aided martensitic steel”, *Metals*, **7**(301), 1-11. <https://doi.org/10.3390/met7080301>.
- Sun, P., Li, S., Yu, G., He, X., Zheng, C. and Ning, W. (2014), “Laser surface hardening of 42CrMo cast steel for obtaining a wide and uniform hardened layer by shaped beams”, *Int. J. Adv. Manuf. Tech.*, **70**, 787-796. <https://doi.org/10.1007/s00170-013-5292-3>.
- Sundqvist, J., Manninen, T., Heikkinen, H.P., Anttila, S. and Kaplan, A.F.H. (2018), “Laser surface hardening of 11% Cr ferritic stainless steel and its sensitization behaviour”, *Surf. Coat. Tech.*, **344**, 673-679. <https://doi.org/10.1016/j.surfcoat.2018.04.002>.
- Tewary, N.K., Syed, B., Ghosh, S.K., Kundu, S., Shariff, S.M. and Padmanabham, G. (2014), “Laser surface hardening of 11% Cr ferritic stainless steel and its sensitisation behaviour”, *Mater. Sci. Eng. A*, **606**, 58-67. <http://dx.doi.org/10.1016/j.msea.2014.03.083>.
- Tressia, G., Pereira, J.I., Penagos, J.J., Bortoleto, E., Sinatora, A. (2021), “Effect of in-service work hardening on the sliding wear resistance of a heavy haul rail in the gauge corner”, *Wear.*, **482-483**(203979), 1-13. <https://doi.org/10.1016/j.wear.2021.203979>.
- Tumanski, S. (2011), *Handbook of Magnetic Measurements*, Warsaw University of Technology. Taylor & Francis Group, LLC.
- Xiang, Y., Yu, D., Cao, X., Liu, Y. and Yao, J. (2017), “Effects of thermal plasma surface hardening on wear and damage properties of rail steel”, *Proceedings of the Institution of Mechanical Engineers, Part J: Journal of Engineering Tribology*, **232**(7), 787-796. <https://doi.org/10.1177/2F1350650117729073>.

Zhang, F.C., Lv, B., Wang, T.S., Zheng, C.L., Zhang, M., Luo, H.H., Liu, H. and Xu, A.Y. (2010), "Explosion hardening of Hadfield steel crossing", *Mater. Sci. Tech.*, **26**(2), 223-229. <https://doi.org/10.1179/174328408X363263>.

TK